

Ultraviolet attenuation by dissolved and particulate constituents of first-year ice during late spring in an Arctic polynya

*Claude Belzile*¹

Groupe de Recherche en Environnement Côtier, Institut des Sciences de la Mer de Rimouski, Université du Québec à Rimouski, 310 Allée des Ursulines, Rimouski, Québec G5L 3A1, Canada

Sophia C. Johannessen

Department of Oceanography, Dalhousie University, Halifax, Nova Scotia B3H 4J1, Canada

Michel Gosselin and Serge Demers

Groupe de Recherche en Environnement Côtier, Institut des Sciences de la Mer de Rimouski, Université du Québec à Rimouski, 310 Allée des Ursulines, Rimouski, Québec G5L 3A1, Canada

William L. Miller

Department of Oceanography, Dalhousie University, Halifax, Nova Scotia B3H 4J1, Canada

Abstract

Vertical profiles of ultraviolet radiation (UVR) and photosynthetically available radiation (PAR) were measured under five large ice floes located in the North Water Polynya, northern Baffin Bay, in June 1998. Together with incident irradiance measurements, these profiles were used to assess the irradiance attenuation by the ice and its constituents. We also measured vertical distribution of absorption by colored dissolved organic matter (CDOM) and particulate organic matter (POM) in three melted ice cores. The ice thickness and snow depth varied from 0.5 to 1.3 m and from 1 to 9 cm, respectively. The ice–snow interface was infiltrated by meltwater. About 2–13% of incident UV-B irradiance was transmitted through the snow, ice, and ice algae biomass; transmittance increased to 5–19% for UV-A and to 5–12% for PAR. CDOM and POM contributed significantly to the attenuation of irradiance within the ice. The relatively high UVR transparency found in this study coincided with the seasonal maximum of incident UV irradiance. Hence, the resulting very high UVR:PAR ratio could affect the communities in the sea ice, at the ice–water interface, and in the surface waters underneath the ice cover. In addition, the strong absorption by CDOM found in this high-UVR environment indicates that significant photochemical reactions could occur.

Seasonal or perennial sea ice covers a large portion of the world's high-latitude oceans, the areas most strongly affected by stratospheric ozone depletion and increased exposure to ultraviolet radiation (UVR). Although many studies have examined the penetration and potential effects of ultraviolet-B (UV-B; 280–320 nm) radiation in the Southern Ocean (Tro-dahl and Buckley 1990; Smith et al. 1992; Weiler and Penhale 1994), in this regard, very little is known about the Arctic region. Perovich et al. (1998) published the only mea-

surements to date of UVR transmission through Arctic sea ice.

It is important to understand the penetration of UVR through sea ice because of its potential effect on the sea ice communities and on the photochemical reactions within and underneath the ice. The bottom-ice environment is the habitat of a productive and extensive sea ice microalgal community (review by Cota et al. 1991; Horner et al. 1992; Legendre et al. 1992). Sea ice microalgae contribute significantly to the annual primary productivity in the Arctic (Legendre et al. 1992; Wheeler et al. 1996) and in the Antarctic (Arrigo et al. 1997). Photophysiological studies indicate that the ice algae are adapted to the low light regime prevailing in their environment during their bloom period, which in the Arctic extends from March to June (Cota et al. 1991). Such shade-adapted microalgae are potentially very sensitive to photoinhibition by UVR (Neale et al. 1994; Prézélin et al. 1998). Photochemical oxidation of colored dissolved organic matter (CDOM) provides an important sink for dissolved organic carbon (DOC) in the ocean (Miller 1994). CDOM photochemistry has not been studied in sea ice, so its importance in this environment is still unknown. The concentration of DOC (up to 40 mg carbon [C] L⁻¹; Melnikov and Pavlov 1978; Thomas et al. 1995; Smith et al. 1997) in sea ice can be relatively high when compared with that in the

¹ Present address: Département de biologie, Université Laval, Sainte-Foy, Québec, Canada, G1K 7P4 (claude.belzile@bio.ulaval.ca).

Acknowledgments

We thank M.-È. Garneau and C. Lovejoy for technical assistance, N. Scully for comments on the proposal, and C. J. Mundy for help with ice characterization. We appreciated the support of the officers and crew of the CCGS *Pierre-Radisson*. The comments and suggestions of W. F. Vincent and two referees were of great value and are gratefully acknowledged. This work was supported by grants from NSERC of Canada to M.G., S.D., and W.L.M., and by Fonds FCAR of Québec to M.G. and S.D. This study represents a contribution to the research programs of the International North Water Polynya Study and to the Groupe de Recherche en Environnement Côtier.

underlying seawater (DOC concentrations of up to 2.5 mg C L⁻¹; Wheeler et al. 1996). If there is sufficient UVR present, photochemical reactions might take place within or just beneath the ice.

UVR attenuation by the ice: General considerations—According to Perovich (1993), transmittance, $T(\lambda)$, is the ratio of the downwelling irradiance at the lower surface of the ice, $E_d(z_{ice}, \lambda)$, to the incident irradiance, $E_d(0, \lambda)$. (For convenience, $T(\lambda)$ is expressed as a percentage here). The transmittance depends on the spectral albedo, $\alpha(\lambda)$ —that is, the fraction of $E_d(0, \lambda)$ that is reflected—and on the attenuation of irradiance by snow and ice, according to Beer's Law. The albedo of snow and ice is very high, varying from about 0.5 to almost 1.0, with the lowest values found for melting conditions (Grenfell and Perovich 1984; Perovich et al. 1998). The spectral downwelling diffuse attenuation coefficient, $K_d(\lambda)$ (per meter), combines the effects of scattering and absorption within the medium. Scattering by the snow is mainly a function of the grain size, snow density, and water content, whereas in-ice scattering depends on ice structure (particularly the brine volume) and particle back-scattering (Buckley and Trodahl 1987; Arrigo et al. 1991; Perovich et al. 1998). The absorption of irradiance depends on the absorptivities of pure ice and brine, CDOM, and particulate organic matter (POM) (Warren et al. 1993; Perovich et al. 1998).

Trodahl and Buckley (1990) found that UV-B transmittance through 1.7-m-thick first-year ice in McMurdo Sound decreased from 2–1% to 0.2–0.1% from the end of October to mid-November, as melting progressed. The decrease in transmittance was considered to be the result of the formation of a highly scattering layer subsequent to ice surface drainage. For 1.6 m of snow-covered first-year ice in the Chukchi Sea (71°N), Perovich et al. (1998) also found UV-B transmittance at 320 nm to decrease by an order of magnitude from 0.3% in April to 0.03% in June. In that case, a bloom of ice algae at the bottom of the ice reduced the UVR transmittance, despite a general tendency toward reduced albedo and decreased attenuation in the upper ice. The influence of ice algae on photosynthetically available radiation (PAR) transmission is well known (Palmisano et al. 1987; Arrigo et al. 1991), although the influence of ice algae on UVR transmission is poorly understood. Since CDOM absorbs strongly at shorter wavelengths, it may be a significant factor in the attenuation of UVR through sea ice as well as an important control on UVR attenuation in the Arctic Ocean water column (Gibson et al. 2000).

Irradiance attenuation measurements—UVR and PAR under-ice irradiance profiles were measured on five occasions in June 1998 during the third leg of the International North Water Polynya Study. Polynyas are recurring meso-scale areas of productive open waters surrounded by less productive ice-covered areas (Lewis et al. 1996; Stirling 1997). The North Water (NOW) Polynya is the largest polynya in the Canadian Arctic and occupies Smith Sound and the northern part of Baffin Bay, between Greenland and Ellesmere Island (Lewis et al. 1996). Table 1 gives details about the ice floes studied. The first-year ice floes (>100 m

Table 1. Sampling time, incident PAR at the time of irradiance measurements, location, average (SD) snow depth, average (SD) ice thickness, average (SD) freeboard thickness, percent of ice surface covered by melt ponds, and average (SD) on duplicate filters) chlorophyll a biomass in the bottom 2 cm of the ice at each station. The average ice thickness and freeboard were determined from four to five ice cores taken in the vicinity, and the average snow depth was calculated from three to five measurements near the hole.

Sta.	Date, time	Incident PAR ($\mu\text{E m}^{-2} \text{s}^{-1}$)	Latitude north (°)	Longitude west (°)	Snow depth (cm) (SD)	Ice thickness (m) (SD)	Freeboard (cm) (SD)	Melt ponds (%)	Chl a (mg m^{-2}) (SD)
C31	14 Jun, 1230 h	599	77°00.29	77°12.90	1 (1)	1.13 (0.09)	8 (1)	0	0.59 (0.03)
C32	15 Jun, 1710 h	233	77°00.41	76°48.69	9 (1)	0.50 (0.05)	4 (0)	0	0.24 (0.01)
C54	20 Jun, 1630 h	1,096	76°20.17	71°49.76	3 (1)	0.66 (0.09)	4 (1)	15	0.92 (0.24)
C43	24 Jun, 1215 h	744	76°23.62	77°45.01	6 (1)	1.31 (0.49)	16 (1)	15	0.22 (0.05)
C73	26 Jun, 1315 h	1,048	75°26.25	72°53.15	4 (1)	0.59 (0.08)	3 (0)	5	0.18 (0.05)

in diameter) were from 0.5 to 1.3 m thick and showed little variability in thickness at a given site, except at Sta. C43, where ice deformation was evident. At all sites the ice was flooded, and much of the snow cover (1 to 9 cm thick) had been infiltrated by meltwater. The freeboard was positive at all stations, with 5–12% of the ice thickness above water level, indicating that the flooding of the snow surface was not due to isostatic processes but rather to the relatively warm air temperature prevailing at the time the measurements were made (0.5–1.6°C). There were melt ponds at three sites (Sta. C54, C43, and C73); these melt ponds covered less than 15% of the surface. The maximum depth of the melt ponds was 18 cm, but more typically the depth was ~10 cm. At Sta. C54 and C73 the surface of the melt ponds was refrozen, and 0.5–3 cm of ice covered the water. The ice cover was $\geq 90\%$ at all stations (visual estimate).

Under-ice irradiance profiles were measured using a PUV/GUV542 radiometer (Biospherical Instruments). The PUV542 measured cosine-corrected downwelling UV irradiance at 305, 313, 320, 340, and 380 nm (full bandwidth at half-maximum of 8–10 nm) and cosine-corrected downwelling PAR (400–700 nm). The instrument also recorded depth and temperature. The GUV542, mounted in an unshaded location on the highest deck of the ship, measured cosine-corrected incident irradiance at the same wavelengths as the PUV542. The PUV and GUV gave ~10 simultaneous data points per meter during profiling. Underwater irradiance measurements were corrected for dark current by subtracting the minimum asymptotic value at the bottom of the profile; if a constant minimum was not achieved (for 380 nm and PAR only), the dark correction was obtained by fitting the radiometer with a light-tight Neoprene cap. The PUV radiometer was lowered to a depth of 20–45 m through a hole of 40-cm diameter drilled through sea ice as far from the ice edge as possible (limited by the length of the profiler cable; at Sta. C31 and C32 the holes were 6 and 7 m from open water, respectively, whereas they were 25 m from open water at the three other stations). During each cast, the hole was tightly covered with a wooden board (1 m² in area) to prevent direct solar radiation from entering the water column through the hole.

The percent of incident irradiance at depth, $\%E_d(z, \lambda)$, was calculated, and the in-water $K_d(\lambda)$ was determined from the linear portion of the plots of the natural logarithm of $\%E_d(z, \lambda)$ versus depth. Because of the shading of the profiler (produced by the wooden cover that was placed over the hole on the ice surface) and because of the sensitivity limit of the radiometer, the plots were linear, on average, from 3 to 8 m in the UV-B, from 5 to 16 m in the UV-A, and from 7 to 21 m for PAR. The r^2 of the relationship between $\ln(\%E_d(z, \lambda))$ and depth was always ≥ 0.98 . The retrieval of $K_d(\lambda)$ for an ice-covered water column was accomplished using an approach similar to that taken by previous authors (e.g., Vincent et al. 1998). From the in-water $K_d(\lambda)$ and the ice thickness (z_{ice}), the percent of incident irradiance just below the ice, $\%E_d(z_{ice}, \lambda)$ (equivalent to the transmittance expressed in percentage), can be calculated as follows:

$$\%E_d(z_{ice}, \lambda) = \%T(\lambda) = \exp[-K_d(\lambda)z_{ice} + y] \quad (1)$$

where y is the intercept of the plots of the natural logarithm

of $\%E_d(z, \lambda)$ versus depth. Because the 0-m depth of the profiler was set at the piezometric water level in the hole, the freeboard thickness (the distance between the ice surface and sea level) was subtracted from z_{ice} (Table 1) in the calculations.

The reconstructed profiles obtained with this method are representative of an unaltered ice sheet, and the $\%T(\lambda)$ values integrate the spatial variability of snow and ice cover and ice algal biomass over a region of a few tens of square meters. The water column estimates of $K_d(\lambda)$ from these profiles were within 1–10% of values from profiles within nearby open water. The similarity of the results indicated that neither the covered hole in the ice nor the nearby ice-free water influenced markedly the $K_d(\lambda)$ measured under the ice. Moreover, substituting the $K_d(\lambda)$ of the ice-free water column for the under-ice $K_d(\lambda)$ in Eq. 1 would change the resulting transmittance by less than 0.3% (11.7 versus 11.4% for $\%T(305)$ at Sta. C73). Extrapolation of the linear part of each plot of $\ln(\%E_d(z, \lambda))$ versus depth to the lower ice surface can thus accurately assess irradiance attenuation by the ice and its components, although positioning an under-ice radiometer (using divers or a remotely operated system) would give a more direct estimate of under-ice irradiance and a better resolution of its fine horizontal variability.

Measurement of dissolved and particulate constituents—Ice cores were taken with a MARK II coring system (9-cm internal diameter; Kovacs Enterprise) at Sta. C32, C43, and C54, close to the holes used for the irradiance profiles. Each core was cut into short sections, stored in plastic Ziploc bags in the dark, and thawed overnight at 5°C. About 100 ml of each melted sample was vacuum-filtered through a 25-mm Whatman GF/F filter and then through a 0.2- μm Schleider and Schuell Nylon 66 filter. The GF/F filters were stored at -80°C for later measurement of spectral absorption by POM. CDOM absorptivity, $a_{CDOM}(\lambda)$ (per meter), was measured immediately in the 0.2- μm filtrate using a 10-cm quartz flow cell in a Hewlett Packard HP8453 diode array spectrophotometer. Absorbance of particles concentrated onto the GF/F filters, $A_{filter}(\lambda)$, was measured over the spectral range of 380 to 750 nm, according to the method of Bricaud and Stramski (1990), using a Perkin-Elmer Lambda 12 UV-Vis spectrophotometer equipped with a 50-mm integrating sphere (Labsphere RSA-PE-20). Absorptivity, $a_{POM}(\lambda)$ (per meter), was calculated from the $A_{filter}(\lambda)$ according to the method of Cleveland and Weidemann (1993), and the contribution of extractable pigments was measured using absolute methanol as a solvent (Bricaud and Stramski 1990). The algorithm of Cleveland and Weidemann (1993) was preferred over the more commonly used one of Bricaud and Stramski (1990) because the latter is not valid for A_{filter} of < 0.2 ; in the upper sections of ice cores, the $A_{filter}(\lambda)$ was often < 0.1 . The absorptivity of CDOM and POM in the melted samples was converted to in situ absorptivity by correcting for ice expansion using an ice expansion factor of 1.1 (after Warren et al. 1993, and from the ratio of the density of seawater to that of sea ice). For chlorophyll *a* (Chl *a*) determination, the lowest 2 cm of three to five ice cores (different cores from those used for absorptivity measurements) was cut and melted in 0.2- μm -filtered surface sea-

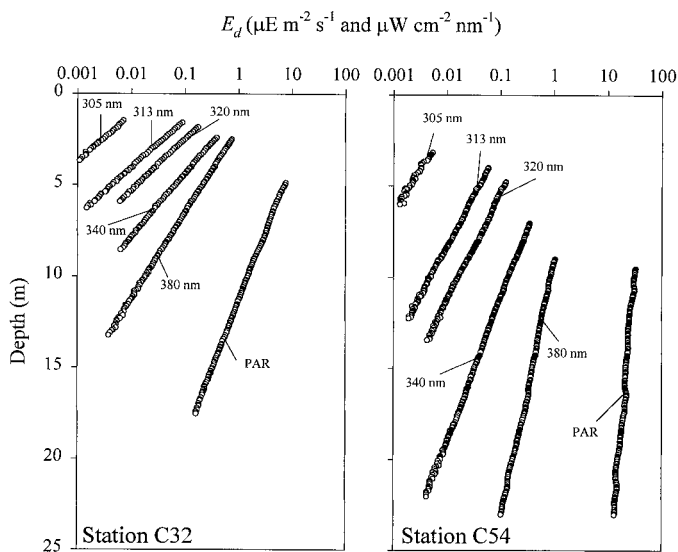


Fig. 1. Typical profiles of PAR ($\mu\text{E m}^{-2} \text{s}^{-1}$) and UVR ($\mu\text{W cm}^{-2} \text{nm}^{-1}$) penetration through the water column under the ice at Sta. C32 with relatively high attenuation and Sta. C54 with low attenuation. The data points shown are those considered for the $K_d(\lambda)$ determination.

water in order to minimize osmotic stresses. Samples were filtered in duplicate onto GF/F filters, and concentrations of Chl *a* were determined on a R010 Turner Designs fluorometer after 24-h extraction in 90% acetone at 4°C (without grinding) (Parsons et al. 1984).

Irradiance attenuation under the ice—Figure 1 shows the typical penetration of irradiance through the water column at two stations—C54, which shows low attenuation, and C32, which shows relatively high attenuation. For the depth intervals considered, only very small changes in the slope of $\ln(E_d(z, \lambda))$ versus depth were observed. These small changes may be due to different water masses. For example, the temperature profile at Sta. C54 shows a sharp increase around 16 m, which corresponds to a small slope change that can be seen in Fig. 1. Figure 2 shows the in-water $K_d(\lambda)$ at each ice-covered site. There were important differences in the attenuation of E_d between the stations, as the water was less transparent at the three nearshore stations (C31, C32, and C43). The depth of 1% surface PAR in the absence of ice varies from 14 m at Sta. C31 to 71 m at Sta. C54; the depth of 1% surface UV-B at 320 nm varies from 6 to 12 m.

Irradiance transmission through the snow, ice, and algal layer—Figure 3 shows the spectral transmittance of UVR and PAR through the ice sheet, as calculated from Eq. 1. About 2–13% of UV-B irradiance at 305, 313, and 320 nm was transmitted through the snow, ice, and algal layers; %*T* increased to 5–19% for UV-A at 340 and 380 nm and to 5–12% for PAR. At all stations, the maximum %*T* was at 380 nm, %*T* decreased approximately linearly with decreasing wavelength, and %*T*(PAR) was lower than the %*T* at 340 and 380 nm. The two stations with the highest %*T*, C73 and C32, were those with the thinnest ice (0.59 and 0.50 m,

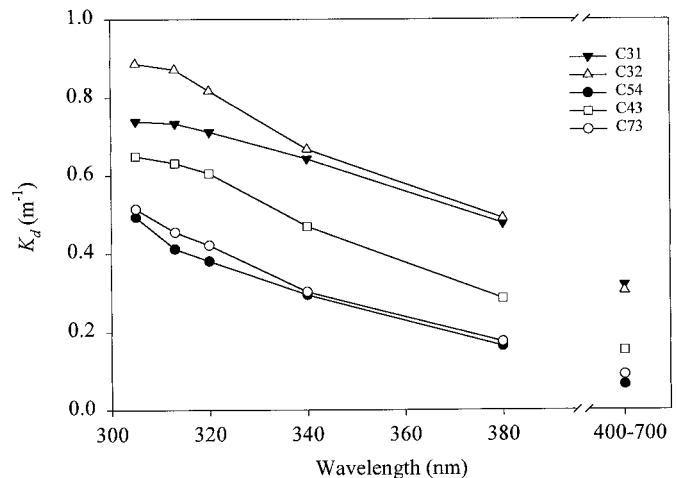


Fig. 2. $K_d(\lambda)$ of the water column under the ice at each station.

respectively; Table 1). The ice was thickest at Sta. C31 and C43 (1.13 and 1.31 m, respectively), which showed the lowest %*T*. Sta. C54, which also showed low %*T*, had an intermediate ice thickness (0.66 m) but the highest Chl *a* concentration at the bottom of the ice (0.92 mg m^{-2} ; Table 1).

Absorption by CDOM and POM—CDOM absorptivity spectra for all three stations are shown in Fig. 4. Superimposed on the usual exponential decay of a_{CDOM} with increasing wavelength, some of the spectra measured in meltwater from the NOW Polynya ice cores showed small slope changes that are often associated with biologically labile organic matter. Except at Sta. C43, the bottom sections were the more colored, supporting the findings of Thomas et al. (1995), who showed that a significant proportion of the dissolved organic matter in sea ice came from decomposition or grazing of ice algae. At Sta. C54, for which a water sample was taken, the magnitude of

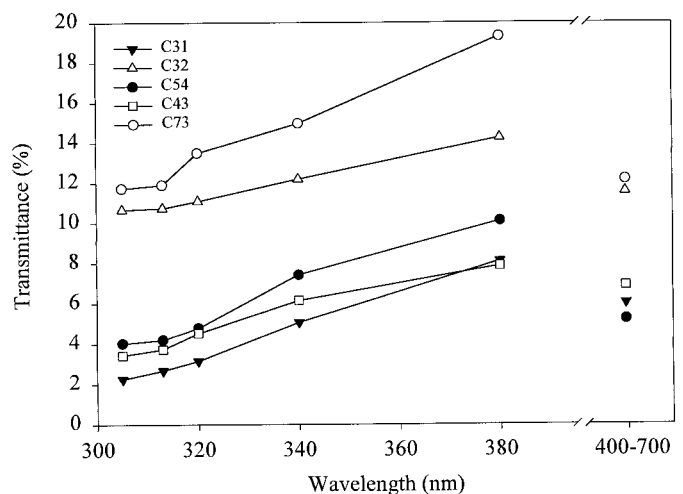


Fig. 3. Spectral transmittance of UVR and PAR irradiance through the ice. The transmittance values presented correspond to the percent of surface irradiance under the ice after transmission through the snow, ice, and ice algae layers.

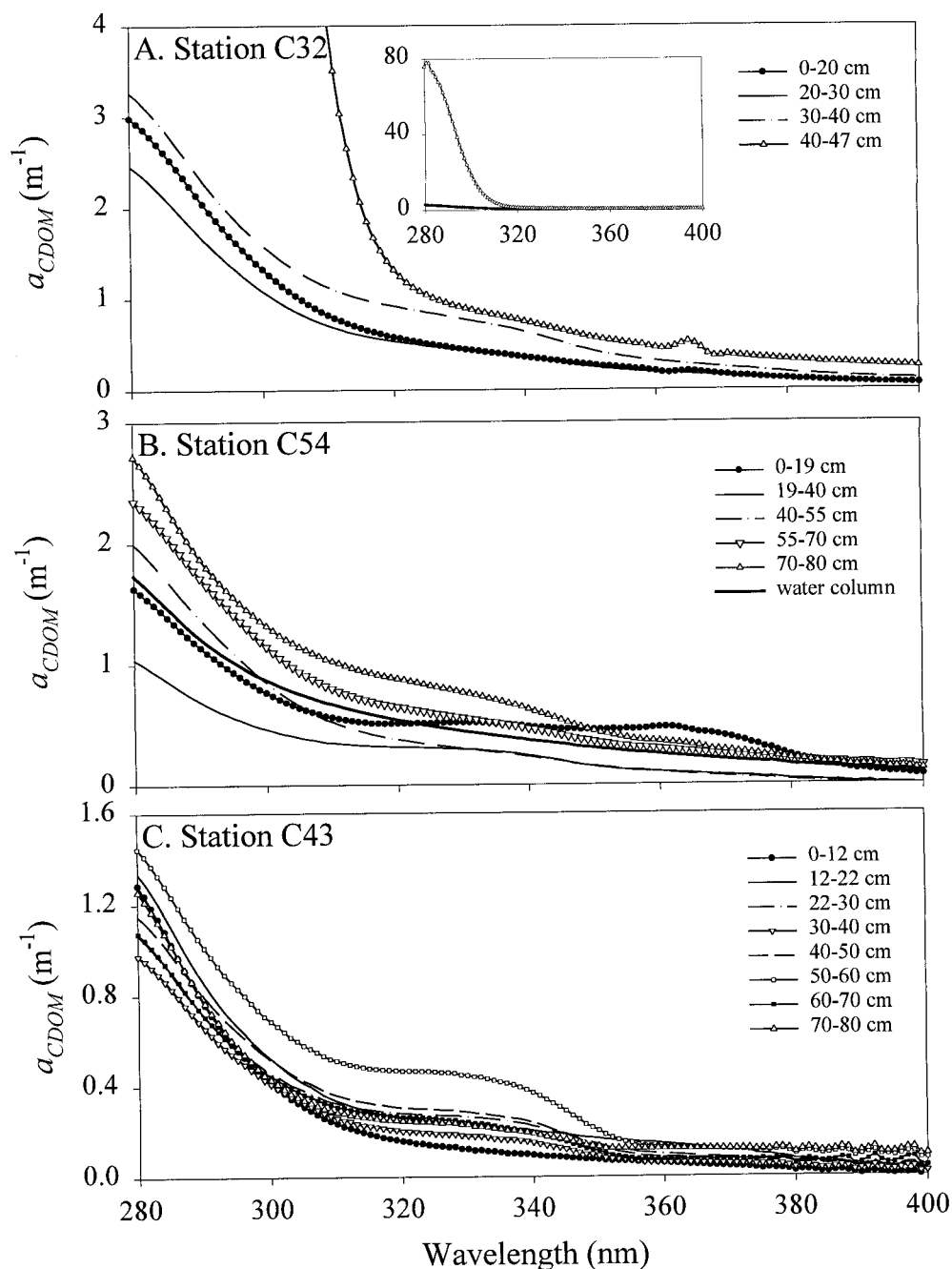


Fig. 4. Spectra of UV absorptivity by CDOM in melted ice sections and underlying water column from Sta. (A) C32, (B) C54, and (C) C43. The insert in (A) shows the high absorptivity found in the bottom section.

$a_{CDOM}(UV)$ in the top sections of the ice was similar to that in the underlying surface water. Near the bottom of the core, the a_{CDOM} was higher than that in the water, which is consistent with earlier suggestions that DOC was concentrated in sea ice (Melnikov and Pavlov 1978). In the bottom section of core C32, a_{CDOM} in the UV-B was more than an order of magnitude higher than that in overlying sections and reached values similar to those found in highly colored lakes. The spectrum of the surface ice samples from Sta. C54 shows a distinctive shoulder from 320 to

380 nm; this shoulder may be associated with mycosporine-like amino acids (MAAs) (Karentz et al. 1991), which are thought to shield marine organisms from UV. Microalgae are known to grow at the upper surface of the ice, especially during the melting season (Horner et al. 1992), and MAAs would help to protect them from the high UVR prevailing at this time of year. Compared to the water column value, a_{CDOM} is surprisingly high in the sea ice. With such strong absorption by CDOM in a high-UVR environment, it is possible that photochemical reactions are

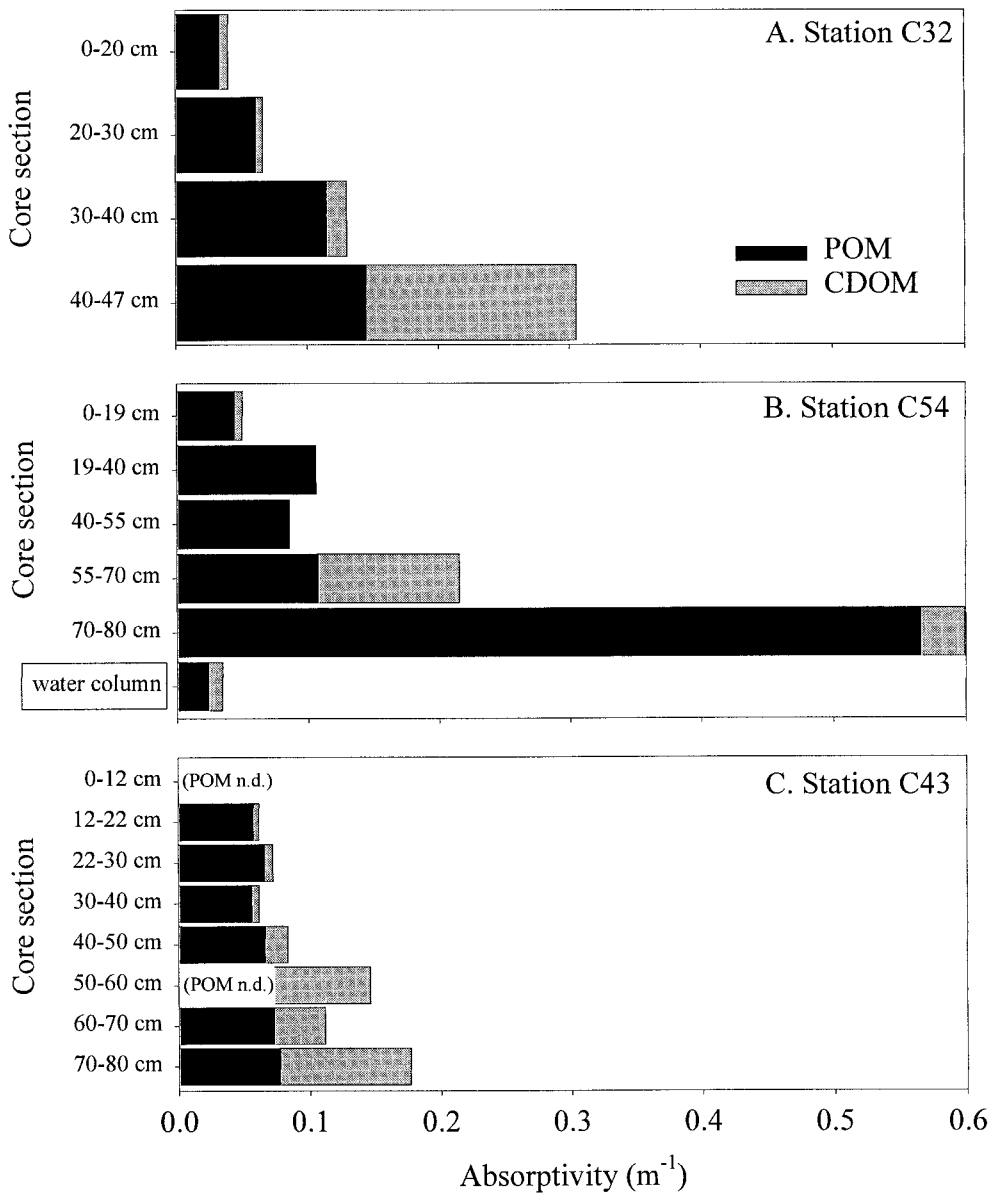


Fig. 5. Vertical variation of in-ice POM and CDOM absorptivities integrated over the PAR range at Sta. (A) C32, (B) C54, and (C) C43. Absorptivity in the underlying surface water at Sta. C54 is also shown. Note that the bars represent different section thickness. POM n.d. = no data available.

occurring at rates comparable to those observed in the upper water column of other oceanic systems.

CDOM and POM also contributed to the absorption of PAR at these three sites. Figure 5 shows the vertical variation of a_{POM} and a_{CDOM} integrated over the PAR range for sections of the cores. In all cases, a_{POM} was highest in the bottom sections, but only Sta. C54 clearly showed the typical Chl *a* absorption peaks at 440 and 665 nm. In all other sections, a_{POM} increased toward shorter wavelengths. Except for the bottom section of Sta. C54, where 83% of a_{POM} was represented by pigments extractable in methanol, most of the a_{POM} was nonextractable. That residual absorption after methanol extraction is often referred to as “detrital matter

absorption” (Bricaud and Stramski 1990), although it also includes the absorption by nonextractable pigments (phycobilins), heterotrophic cells, and bleached algal cells. Although a_{CDOM} in the PAR range was very low in the top sections of the ice, the a_{CDOM} in the bottom sections was sometimes as high as the a_{POM} . The total absorption by organic matter (a_{OM} , the sum of a_{POM} and a_{CDOM}) was three to twelve times higher at the bottom of the ice than at the surface (Fig. 5). Interestingly, PAR absorption due to CDOM and POM at Sta. C54 was 17 times higher in the bottom section of the ice than in the underlying water; integrated over the whole ice sheet, the a_{OM} was still four times higher than in the water. Table 2 shows average a_{OM} for specific

Table 2. Average absorptivity in the ice due to CDOM and POM, $a_{OM}(\lambda)$, at wavelengths of interest. a_{OM} values in surface waters at Sta. C54 are also presented for comparison.

Sta.	$a_{OM}(380)$ (m^{-1})	$a_{OM}(440)$ (m^{-1})	$a_{OM}(670)$ (m^{-1})
C32 ice	0.45	0.20	0.04
C54 ice	0.46	0.33	0.14
C54 surface waters	0.22	0.10	0.02
C43 ice	0.22	0.16	0.06

wavelengths in UV-A and PAR, for which both CDOM and POM absorptivities are available. The in-ice absorptivity was always greater than or equal to that measured in surface waters at Sta. C54 and was higher at 380 nm than at wavelengths corresponding to absorption peaks of algae (440 and 670 nm).

Modeled irradiance transmission through sea ice—In a major contribution to the optical modeling of sea ice, Maffione et al. (1998) measured the beam spread function of sea ice in the Chuckchi Sea. They equated the results of diffusion theory with asymptotic radiative transfer theory in order to relate the asymptotic attenuation coefficient, K_{∞} (per meter), to the inherent optical properties (IOPs) of sea ice. In their calculations of the beam attenuation coefficient, c (per meter), as a function of K_{∞} , they assumed that the contribution of the microalgal cells embedded in the ice to $a(670)$ was at most $0.3 m^{-1}$. As Table 2 shows, the measured $a_{OM}(670)$ integrated over the whole ice sheet is lower than the maximum value used by Maffione et al. (1998). However, that was not the case at the bottom of the ice, where both a_{CDOM} and a_{POM} tended to be the higher and represented precisely where the asymptotic state should be approached. Effectively, in the bottom 10 cm of the ice at Sta. C54, $a(670)$ reached $1.10 m^{-1}$, which gave $c \cong 20 m^{-1}$ for $K_{\infty} = 2.5 m^{-1}$, compared with $c \cong 50 m^{-1}$, as reported by Maffione et al. (1998). This implies that the single-scattering albedo, ω_0 , falls below 0.95 for $K_{\infty} \cong 2.5 m^{-1}$ and could be as low as 0.91 for $K_{\infty} = 2.0 m^{-1}$, which indicates that the diffusion approximation (Maffione 1998) might not be valid for describing light propagation in the asymptotic limit of organic matter-enriched sea ice. Despite the recognized highly scattering nature of sea ice, our results show that absorption by ice algae-associated organic matter also plays a significant role in irradiance attenuation.

Kirk (1994) showed from Monte Carlo radiative transfer calculations of highly turbid waters that K_{∞} could be satisfactorily related to a and to the scattering coefficient, b (per meter), by the following equation:

$$K_{\infty} = (a^2 + Gab)^{1/2} \quad (2)$$

where G is a free parameter found to depend on the shape of the scattering phase function. Kirk (1994) reported the value of $G = 0.233$ for the highly scattering cases. Maffione (1998) found a very similar value (0.238) under the diffusion approximation and showed that Eq. 2 was valid for sea ice. From their beam spread function measurements, Maffione et al. (1998) suggested that the asymptotic radiance distribution

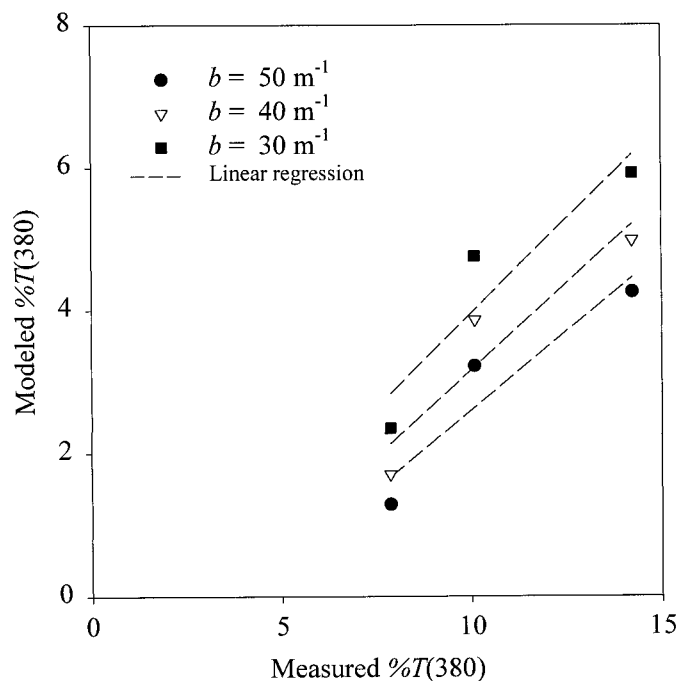


Fig. 6. Relationship between measured and modeled transmittance at 380 nm for likely values of scattering coefficient, b . Note that 380 nm is the only wavelength for which both in-ice absorptivity and transmittance were measured.

was closely approached in sea ice for a path length of >30 cm. Using the measured $a_{OM}(380)$ (Table 2), the $a_{pure\ ice}(380)$ from Perovich and Govoni (1991), and $G = 0.233$, the K_{∞} for each ice core was calculated with Eq. 2 for likely values for b of 30, 40, and $50 m^{-1}$. The resulting $K_{\infty}(380)$ varied from 1.6 to $2.6 m^{-1}$, depending on the station and the value of b used. Using an albedo of 0.8 (given by Perovich et al. [1998] for 6 cm of melting snow over 1.6 m of sea ice, conditions resembling those prevailing during this study), the K_{∞} calculated using Eq. 2, and the ice thickness at each station (Table 1), the transmittance at 380 nm was modeled for $b = 30, 40,$ and $50 m^{-1}$. In the absence of an appropriate value for the snow cover, the 3–9 cm of snow over the ice was assumed to have the same K_{∞} as the sea ice. Figure 6 shows the resulting relationships between measured and modeled transmittance. The good correlation between observed and modeled values is remarkable considering that $a_{OM}(380)$ from a single core is related to bulk transmittance at the station. However, the measured $\%T$ was, on average, 2.6 and 4.2 times higher than the modeled $\%T$ for $b = 30 m^{-1}$ and $b = 50 m^{-1}$, respectively. Again, horizontal variability of ice- and snow-cover characteristics, including the extent of melt ponds, may explain part of this discrepancy. Specifically, the low albedo of melt ponds (0.33 for a 10-cm-deep melt pond; Perovich et al. 1998) may decrease the overall albedo of the surface. Using an albedo of 0.6, rather than one of 0.8, in order to account for the melt ponds present at Sta. C54 and C43 (Table 1), a close to 1:1 ratio is found between measured and modeled transmittance for $b = 30 m^{-1}$. Note, however, that Eq. 2 may not be strictly valid for 380-nm UV-A irradiance. More simultaneous in-ice ab-

sorptivity and transmittance measurements are needed to evaluate thoroughly the model performance and to derive sea ice IOPs from these measurements. To our knowledge, the results presented here represent the first published attempt to relate quantitatively measured in-ice absorptivity and transmittance.

Implications for ice algae and the carbon budget of the Arctic—Important differences exist between the Antarctic and the Arctic in terms of the modifications of ice optical properties as spring progresses. Whereas surface melting is a major factor in the summer disappearance of Arctic ice, Antarctic ice is characterized by minimal surface melting and an absence of melt ponds (Maykut 1985). The increased turbidity of Antarctic ice in late spring as a result of the drainage of brine from the surface of the ice causes a 10-fold reduction of UVR transmission from early spring values (Trodahl and Buckley 1990). During the present study, from mid- to late June, the ice was covered by wet or melting snow, and melt ponds were present at three stations. These conditions result in both reduced albedo and lower scattering (Perovich et al. 1998), leading to higher overall transparency to UVR. Another factor explaining the high UVR transmittance is that the 0.5–1.3-m-thick ice was thinner than that studied by Trodahl and Buckley (1990) and Perovich et al. (1998). Also, the ice algae biomass measured at the bottom of the ice was approximately one order of magnitude lower than that found in April and May (Michel Gosselin, Christine Michel unpubl. data), presumably allowing a higher proportion of UVR to be transmitted.

A comparison of the bottom-ice environment and the water column reveals that the ice cover may exacerbate the biological impact of UVR by increasing the ratio of UVR to PAR. At Sta. C54, for example, the algae at the ice–water interface were exposed to at least 4% of the incident UV-B and 5% of the incident PAR (Fig. 3). In an equivalent ice-free water column, 4% of incident UV-B would remain at 7.5 m, but at that depth, there would still be 62% of the incident PAR. The difference arises mainly from the high PAR attenuation by the ice algae and associated organic matter (Fig. 5 and Table 2). Thus, when compared to the ice-free water column, the bottom-ice environment is a relatively high-UV-B, low-PAR environment. That is particularly important because the balance between UV-B damage and repair is not only a function of the absolute intensities but also depends on the ratio of UV-B to longer wavelengths (Vincent and Roy 1993). Shade-adapted ice algae are highly susceptible to UVR damage (Neale et al. 1994; Prézélin et al. 1998). Moreover, the sea ice provides a vertically stable surface for microalgal growth, removing the influence of vertical mixing on photoacclimation and repair processes of UVR damage (Vincent and Roy 1993).

Gibson et al. (2000) have shown that the Arctic Ocean is strongly influenced by riverine inputs of CDOM. They showed that shifts in CDOM loading through climate change or changes in ocean circulation can cause variations in biological UVR exposure, variations that are much greater in magnitude than are ozone-related effects. Climate change may also modify UVR exposure through its influence on snow and ice cover via changes in temperature and precip-

itation. Given the relatively high UVR transmittance and high incident UVR during the melt season, changes in the timing of melt would strongly influence the exposure to UVR. Considering the important contribution of the bottom-ice assemblage to the carbon budget in the Arctic Ocean, the findings presented here are of ecological interest and indicate the need for evaluating the impact of UVR on the ice community and on the photochemistry within the ice.

References

- ARRIGO, K. R., C. W. SULLIVAN, AND J. N. KREMER. 1991. A bio-optical model of Antarctic sea ice. *J. Geophys. Res.* **96**: 10581–10592.
- , D. L. WORTHEN, M. P. LIZOTTE, P. DIXON, AND G. DIECKMANN. 1997. Primary production in Antarctic sea ice. *Science* **276**: 394–397.
- BRICAUD, A., AND D. STRAMSKI. 1990. Spectral absorption coefficients of living phytoplankton and nonalgal biogenous matter: A comparison between the Peru upwelling area and the Sargasso Sea. *Limnol. Oceanogr.* **35**: 562–582.
- BUCKLEY, R. G., AND H. J. TRODAHL. 1987. Scattering and absorption of visible light by sea ice. *Nature* **326**: 867–869.
- CLEVELAND, J. S., AND A. D. WEIDEMANN. 1993. Quantifying absorption by aquatic particles: A multiple scattering correction for glass-fiber filters. *Limnol. Oceanogr.* **38**: 1321–1327.
- COTA, G. F., L. LEGENDRE, M. GOSSELIN, AND R. G. INGRAM. 1991. Ecology of bottom ice algae: I. Environmental controls and variability. *J. Mar. Syst.* **2**: 257–277.
- GIBSON, J. A. E., W. F. VINCENT, B. NIEKE, AND R. PIENITZ. 2000. Control of biological exposure to UV radiation in the Arctic Ocean: Comparison of the roles of ozone and riverine dissolved organic matter. *Arctic*. In press.
- GRENFELL, T. C., AND D. K. PEROVICH. 1984. Spectral albedos of sea ice and incident solar irradiance in the southern Beaufort Sea. *J. Geophys. Res.* **89**: 3573–3580.
- HORNER, R., AND OTHERS. 1992. Ecology of sea ice biota. 1. Habitat, terminology and methodology. *Polar Biol.* **12**: 417–427.
- KARENTZ, D., F. S. MCEUEN, M. C. LAND, AND W. C. DUNLAP. 1991. Survey of mycosporine-like amino acid compounds in Antarctic marine organisms: Potential protection from ultraviolet exposure. *Mar. Biol.* **108**: 157–166.
- KIRK, J. T. O. 1994. Characteristics of the light field in highly turbid waters: A Monte Carlo study. *Limnol. Oceanogr.* **39**: 702–706.
- LEGENDRE, L., AND OTHERS. 1992. Ecology of sea ice biota. 2. Global significance. *Polar Biol.* **12**: 429–444.
- LEWIS, E. L., D. PONTON, L. LEGENDRE, AND B. LEBLANC. 1996. Springtime sensible heat, nutrients and phytoplankton in the Northwater Polynya, Canadian Arctic. *Cont. Shelf Res.* **16**: 1775–1792.
- MAFFIONE, R. A. 1998. Theoretical developments on the optical properties of highly turbid waters and sea ice. *Limnol. Oceanogr.* **43**: 29–33.
- , J. M. VOSS, AND C. D. MOBLEY. 1998. Theory and measurements of the complete beam spread function of sea ice. *Limnol. Oceanogr.* **43**: 34–43.
- MAYKUT, G. A. 1985. The ice environment, p. 21–82. *In* R. A. Horner [ed.], *Sea ice biota*. CRC Press.
- MELNIKOV, I. A., AND G. L. PAVLOV. 1978. Characteristics of organic carbon distributions in the waters and ice of the Arctic Basin. *Oceanology* **18**: 163–167.
- MILLER, W. L. 1994. Recent advances in the photochemistry of natural dissolved organic matter, p. 111–127. *In* G. R. Helz and D. G. Crosby [eds.], *Aquatic and surface photochemistry*. CRC Press.

- NEALE, P. J., M. P. LESSER, AND J. J. CULLEN. 1994. Effects of ultraviolet radiation on the photosynthesis of phytoplankton in the vicinity of McMurdo Station, Antarctica. *Antarct. Res. Ser.* **62**: 125–142.
- PALMISANO, A. C., J. B. SOOHOO, R. L. MOE, AND C. W. SULLIVAN. 1987. Sea ice microbial communities. VII. Changes in under-ice spectral irradiance during the development of Antarctic sea ice microbial communities. *Mar. Ecol. Prog. Ser.* **35**: 165–173.
- PARSONS, T. R., Y. MAITA, AND C. M. LALLI. 1984. A manual of chemical and biological methods for seawater analysis. Pergamon Press.
- PEROVICH, D. K. 1993. A theoretical model of ultraviolet light transmission through Antarctic sea ice. *J. Geophys. Res.* **98**: 22579–22587.
- , AND J. W. GOVONI. 1991. Absorption coefficients of ice from 250 to 400 nm. *Geophys. Res. Lett.* **18**: 1233–1235.
- , C. S. ROESLER, AND W. S. PEGAU. 1998. Variability in Arctic sea ice optical properties. *J. Geophys. Res.* **103**: 1193–1208.
- PRÉZELIN, B. B., M. A. MOLINE, AND H. A. MATLICK. 1998. Ice-colors '93: Spectral UV radiation effects on Antarctic frazil ice algae, p. 45–83. *In* M. P. Lizotte and K. R. Arrigo [eds.], *Antarctic sea ice: Biological processes, interactions and variability*. *Antarct. Res. Ser.*, Vol 73, American Geophysical Union.
- SMITH, R. C., AND OTHERS. 1992. Ozone depletion: Ultraviolet radiation and phytoplankton biology in Antarctic waters. *Science* **255**: 952–958.
- SMITH, R. E. H., M. GOSSELIN, S. KUDOH, B. ROBINEAU, AND S. TAGUCHI. 1997. DOC and its relationship to algae in bottom ice communities. *J. Mar. Syst.* **11**: 71–80.
- STIRLING, I. 1997. The importance of polynyas, ice edges, and leads to marine mammals and birds. *J. Mar. Syst.* **10**: 9–21.
- THOMAS, D. N., R. J. LARA, H. EICKEN, G. KATTNER, AND A. SKOOG. 1995. Dissolved organic matter in Arctic multi-year sea ice during winter: Major components and relationship to ice characteristics. *Polar Biol.* **15**: 477–483.
- TRODAHL, H. J., AND R. G. BUCKLEY. 1990. Enhanced ultraviolet transmission of Antarctic sea ice during the austral spring. *Geophys. Res. Lett.* **17**: 2177–2179.
- VINCENT, W. F., R. REA, I. LAURION, C. HOWARD-WILLIAMS, AND J. C. PRISCU. 1998. Transparency of Antarctic ice-covered lakes to solar UV radiation. *Limnol. Oceanogr.* **43**: 618–624.
- , AND S. ROY. 1993. Solar ultraviolet-B radiation and aquatic primary production: Damage, protection, and recovery. *Environ. Rev.* **1**: 1–12.
- WARREN, S. G., C. S. ROESLER, V. I. MORGAN, R. E. BRANDT, I. D. GOODWIN, AND I. ALLISON. 1993. Green icebergs formed by freezing of organic-rich seawater at the base of Antarctic ice shelves. *J. Geophys. Res.* **98**: 6921–6928.
- WEILER, S., AND P. PENHALE. 1994. Ultraviolet radiation in Antarctica: Measurements and biological effects. *Antarct. Res. Ser.*, Vol 62, American Geophysical Union.
- WHEELER, P. A., M. GOSSELIN, E. SHERR, D. THIBAUT, D. L. KIRCHMAN, R. BENNER, AND T. E. WHITLEDGE. 1996. Active cycling of organic carbon in the central Arctic Ocean. *Nature* **380**: 697–699.

Received: 20 July 1999

Accepted: 3 May 2000

Amended: 31 May 2000